Comparison of the Direct Supervised Classification and Segment Mean Shift Classification: A Case Study of Hetauda Sub-Metropolitan City of Nepal

Menaka Hamal[1], Prof. Shahnawaz (Ph.D.)[2]
menakahamal@gmail.com, shahnawaz.shahnawaz@plus.ac.at
[1]Nutan GeoEnvironmental Consultancy Pvt. Ltd, [2]University of Salzburg

KEYWORDS

Segment Mean Shift, Supervised Classification, Land Use Land Cover, Training Samples, Point Sampling

ABSTRACT

Comparison between Land Use Land Cover (LULC) classification and methods is a common practice to assess their suitability and reliability in specific areas. In the case of Hetauda Sub-Metropolitan City in Nepal, Sentinel-2B satellite imagery was utilized to evaluate the accuracy of LULC classification through both direct supervised classification and segment mean shift classification. Direct supervised classification was conducted in ERDAS Imagine, while segment mean shift classification was performed in ArcGIS to identify six LULC classes: forest, agriculture, built-up area, bare area, grassland, and waterbody. Pre-processing steps such as layer stacking, mosaicking, data extraction, atmospheric and radiometric correction were employed to enhance the imagery. Training samples were chosen via visual interpretation based on local knowledge to train the Maximum Likelihood Classifier (MLC). The results revealed that the segment mean shift method achieved the highest overall accuracy at 90%, whereas direct supervised classification yielded 85%. Furthermore, kappa statistics indicated a strong level of agreement, with segment mean shift scoring the highest at 0.88 and direct supervised classification at 0.81. Individual class accuracies varied, with forest classification being the most reliable at 98% and waterbody classification at 71%. Overall, the segment mean shift method was deemed more accurate and suitable than the pixel-based direct supervised classification for LULC classification in Hetauda Sub-Metropolitan City, Nepal.

1. INTRODUCTION

LULC classification utilizing satellite imagery has been widely practiced on both local and global scales (Belward & Skøien, 2015). Advancements in sensor technology worldwide, coupled with the accessibility of various satellite images and user-friendly spatial analysis tools, have heightened interest and improved the accuracy of LULC information extraction (Phiri & Morgenroth, 2017). Among the techniques employed, supervised classification stands out, allowing users to select sample pixels based on their prior knowledge of the area. These samples serve to train other pixels, enabling the identification of the closest LULC information across the entire

study area (Enderle & Robert, 2005; Lillesand et al., 2015). Recently, the segment mean shift classification, facilitated by ArcGIS, has gained popularity. This approach, recognized for its robustness in feature space analysis (Comaniciu & Meer, 2002), involves grouping pixels based on similar characteristics from adjacent pixels, resulting in super pixels or segments. These super pixels are then classified, either supervised or unsupervised, depending on the study's objectives (ESRI, n.d.-a).

Access to satellite imagery varies, with free options often offering lower resolution and limited temporal coverage (Hegarty-Craver et al., 2020). The Sentinel-2 datasets, however, provide an alternative as they are freely available every five days and relatively high resolution compared to other open-source options. These datasets encompass 13 spectral bands with varying spatial resolutions: four bands at 10 meters, six at 20 meters, and three at 60 meters, with a 12-bit radiometric resolution allowing for a potential range of brightness levels from 0 to 4095 (ESA, n.d.). Ensuring the reliability of remotely sensed maps prior to their application is crucial in image classification (Congalton, 2001). The assessment can be done through comparisons with reference points from the original imagery, ground truth point collection (Enderle & Robert, 2005), or the author's prior knowledge of the study area. In this study, a stratified random sampling method is adopted to generate reference points. These points are then distributed across each stratum using the Sampling Design Tool to calculate the confusion matrix and kappa statistics, thereby assessing the reliability of the classified maps.

Open-access satellite data, including Landsat, MODIS, ASTER, VIIRS, IKONOS-2, OrbView-3, among others, are obtainable from sources such as the USGS Earth Explorer and various web services. GEOS-R and NOAA-20 data can be acquired from the NOAA web portal, while Sentinel-2A, Sentinel-2B, and similar data are accessible via the ESA open access portal. For data processing and analysis, a range of remote sensing software is available and selected based on the study's requirements (Roy et al., 2017), such as ERDAS Imagine, ArcGIS, eCognition, and so on. While classification can be performed using open-source platforms like QGIS and other programming languages, this study utilized commercial software, specifically ERDAS and ArcGIS. ERDAS, recognized as raster-based software, is widely utilized for extracting information from images and executing multiple geospatial tasks (Intergraph, 2021), particularly renowned for pixel-based classification (Basayigit, 2015). Similarly, ArcGIS facilitates the management and analysis of diverse geographic information, allowing for the visualization of geographical statistics through layer-based maps, and is popular for both pixel and object-based analysis (ESRI, n.d.-a).

In thematic mapping, accuracy assessment holds significant importance, serving as a pivotal step to gauge the reliability of the generated products for subsequent applications (FAO, 2016). As emphasized by Lillesand et al. (2015), "A classification is not complete until its accuracy is assessed." Thus, to ensure the integrity of the classification results, this study adopted a point sampling approach for accuracy assessment. The determination of the desired number of test points was guided by the principle that each class should ideally have ten times the number of test points (MGL, n.d.).

The kappa is one of the commonly used statistics to test the degree of agreement by chance (Viera & Garrett 2005). The values range from 0 to 1 where 0 interprets no agreement between the classified and reference images and 1 gives the classified images and the ground truth images are identical (Cohen, 1960). So, the higher the kappa coefficient, the more accurate the classification is. The level of the agreement depends on the value of Kappa

that gives the percentage reliability of the data. The value 0 to 0.20 gives the 0-4% reliability that interprets no agreement, 0.21 to 0.39 gives 4-15% reliability with the minimal agreement, 0.40 to 0.59 gives 15-35% reliability that interprets the weak level of agreement, 0.60 to 0.79 gives 35-63% reliability with the moderate agreement, 0.80 to 0.90 gives 64-81% reliability interprets the strong level of agreement and above 0.90 gives 82-100% that interprets the almost perfect level of agreement (McHugh, 2012).

Hetauda Sub-Metropolitan City is one of the recently emerged densely populated city due to its strategic location at the convergence of Nepal's historic East West Highway and Tribhuvan Highway, linking the Tarai region with the Kathmandu Valley. The city has witnessed a significant influx of migrants from various regions, including the Tarai, Mountain, Hill, and nearby rural villages, in search of employment opportunities, better education, and improved infrastructure. Rapid urbanization driven by population growth and land demand for construction purposes has led to the conversion of agricultural land into built-up areas. Additionally, natural water bodies have been transformed into ponds for fisheries and other agricultural activities, while forests and grasslands have faced depletion due to infrastructure development. The widening of riverbanks and occurrences of floods during the monsoon season further highlight the dynamic changes in the landscape (GoN, 2017).

This study outlines the significance of observing notable LULC changes within the city. It aims to assess the accuracy of land cover mapping using two distinct approaches: the segment mean shift supervised classification and direct supervised classification methods. The primary objective is to ascertain the current status of LULC in the expanded metropolitan area. The study endeavors to provide valuable insights to guide the formulation of land use policies by governmental and non-governmental organizations. Specifically, it seeks to address inquiries regarding the extent of LULC and, the appropriateness of classification techniques tailored to urban contexts, and the trends in LULC changes over the past decade within the metropolis.

2. METHODOLOGY

2.1 Study area

The Hetauda Sub-Metropolitan City is situated in the southern region of the Makwanpur district within the Bagmati Province of Nepal. The geographic coordinates lie between 27.541940 to 27.32417° N latitude and 85.89083° to 85.1900° E longitude. Spanning an area of 261.58 square kilometers, the elevation within the city ranges from 300 to 1,800 meters above sea level. The sub-metropolis is home to a population of 193576 individuals, comprising 95,678 males and 97898 females, residing in a total of 46566 households (CBS, 2021). The climate and terrain of the city are conducive to agricultural productivity and human habitation. It is located within the inner Terai region, experiences a dominant tropical climate, transitioning into sub-tropical conditions with increasing elevation, and eventually into a lower temperate climate at higher altitudes (DoA, 2018). According to the city profile of 2017, approximately 41.46% of the city is covered by forest, while agricultural land occupies another 41% of the total area. The remaining land includes areas classified as barren, built-up, bush, grasslands, orchards, ponds, sand, and water bodies (GoN, 2017).

2.2 Data acquisition

Two multispectral images from Sentinel-2B covering an area of 100 meters by 100 meters each, acquired on March 31, 2020, from the Copernicus Open Access Hub, specifically located at UTM grid codes – 45 RTL and 45 RUL (ESA, n.d.). The datasets were geo-referenced and orthorectified with UTM 45 N projection. Comprising a total of 13 spectral bands ranging from Visible and Near Infra-Red (VNIR) to Short Wave Infra-Red (SWIR),

four bands with a spatial resolution of 10 meters were selected for the study: blue (456 – 532 nm), green (536 - 582nm), red (646 – 685 nm), and near-infrared (774 – 907 nm) (ESA, 2015).

2.3 Image preprocessing

Image preprocessing techniques were employed to improve the visualization and interpretability of features present in the imagery. Initially, single layers with uniform cell sizes were stacked in Erdas Imagine to create a multi-band image. Subsequently, multiple tiles of the multi-band imagery were merged using the mosaic tool. The mosaic image underwent enhancement to refine image quality. The radiometric calibration was performed to mitigate atmospheric distortion caused by cloud and aerosols. The point spread method was applied to reduce haze and enhance image sharpness. Additionally, the histogram equalization tool was utilized to minimize noise distortion and enhance image features.

2.4 Image segmentation

The image segmentation process was carried out for the segment mean shift supervised classification, following the mean shift approach (ESRI, n.d.-c). Utilizing the Segment Mean Shift tool in ArcGIS, the objects within the processed imagery were grouped into segments based on their shapes, spectral properties, and spatial characteristics. By iteratively adjusting the spectral values within the range of 15.5 to 20, the segments were refined to closely resemble real features within the scene. Ultimately, a spectral value of 18 was determined to be the most suitable for approximating the shape of objects in the imagery. Similarly, a spatial value of 15 was identified as providing the best fit for the objects present in the imagery. Through multiple iterations, the minimum segment size was established at 20, ensuring that super pixels smaller than this threshold merged with their closest neighbor segment (Figure 1).

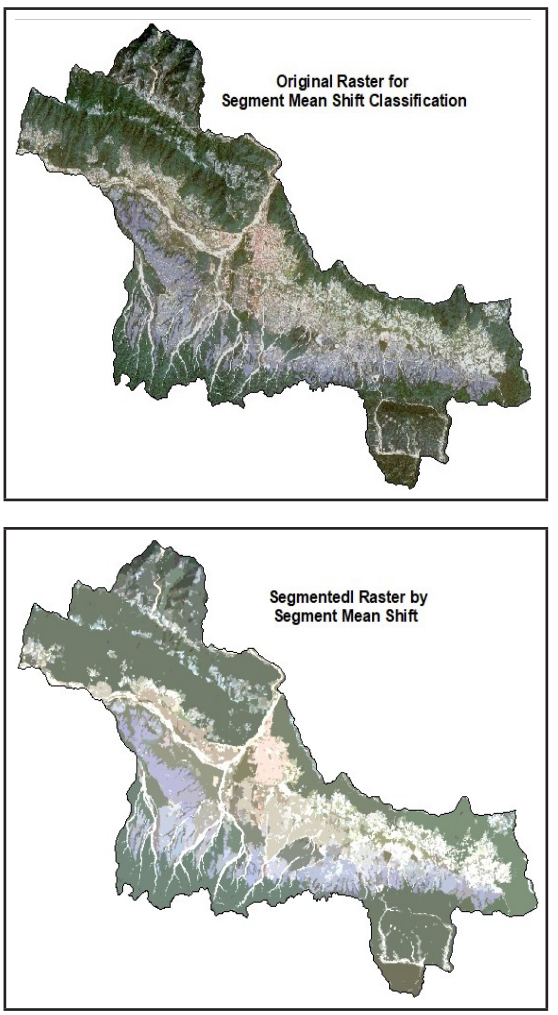

Figure 1: Original and segmented raster

2.5 LULC classification scheme

The LULC classes have been categorized depending on the desired objectives, available features on the image, and applicability of the ground coverage (Ai et al., 2020). The range of classes has been chosen for the LULC classification for a specific area (Basayigit, 2015). This study adhered to the predefined LULC classes utilized in prior land cover assessment by the city. As documented in the City profile of 2017, the classes included barren land, built-up areas, bush, cultivation, forest, grass, orchard, pond, sand, and water

bodies. Building upon a scheme for this study, certain refinements were made to streamline classification processes. Specifically, the pond and water body categories into a water body class, while sand and barren land were consolidated under the barren land category. Furthermore, the bush and grassland designations were merged to form a unified grassland class. Similarly, the cultivation class was relabeled as agriculture. Consequently, the classification scheme employed in this study encompasses six distinct classes: Agriculture, Bare Area, Builtup Area, Forest, Grassland, and Waterbody.

2.6 Training samples

Training samples for the supervised classification must be both representative and complete (Lillesand, et al. 2015). The rule of thumb is that the more samples that can be used in training, the better the statistical representation of each spectral class (ESRI, n.d.-d). Adhering to this rule, the required samples were drawn based on the coverage of the area through visual interpretation using polygon tool in ERDAS across the scene considering the samples are normally distributed for the respective land coverage in the city. Considering the provided data. Based on this, Agriculture, Builtup Area, and Forest classes each have 47 training samples chosen for classification. Bare Area and Waterbody classes are represented by 35 training samples each, while Grassland has 21 samples allocated for training. Following the collection of training samples, a signature file was generated, encompassing essential parameters such as the mean values for each class, the count of pixels, and the variance and covariance matrix for the training class. This signature file served as a crucial input for training the Maximum Likelihood Classifier (MLC), facilitating the classification of pixels throughout the entire imagery based on the established signatures (Figure 2).

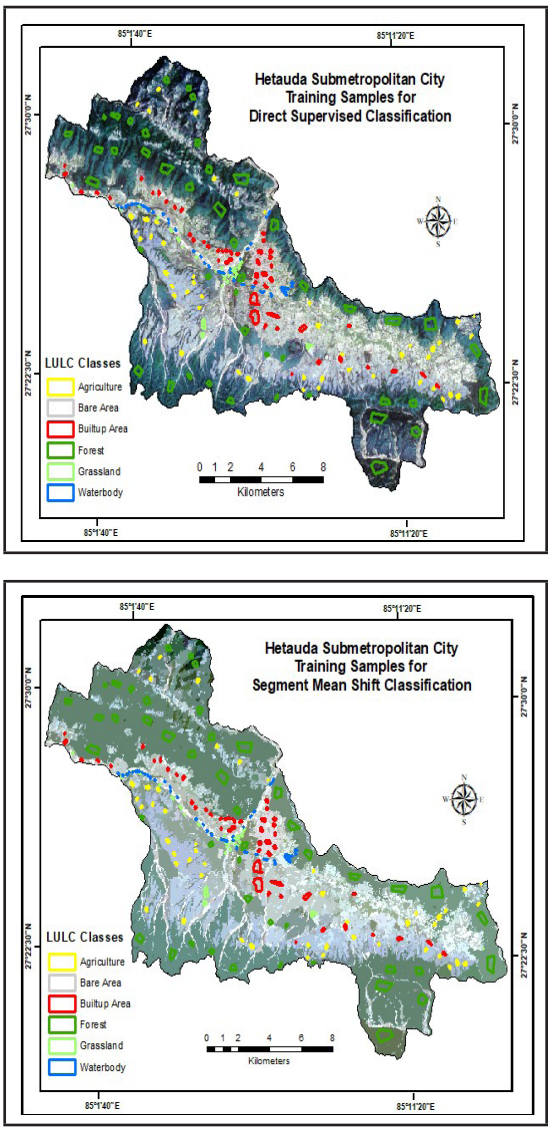

Figure 2: Training samples as thematic classes

2.7 Point sampling and accuracy assessment

To calculate the sample size, all classes were ranked based on their respective area coverage, ranging from lowest to highest. Subsequently, each rank was divided by the total number of ranks and multiplied by the total number of pixels to assign the sample size for each class. Consequently, the total number of pixels amounted to 6*6*10 = 360 for the classified scene (Table 1).

Table 1. A sample size of test points for accuracy assessment

Class	Ratio	Sample size
Agriculture	5	5/21*360 = 86
Bare Area	4	4/21*360 = 69
Built-up Area	3	3/21*360 = 51
Forest	6	6/21*360 =103
Grass	2	2/21*360 = 34
Waterbody	1	1/21*360 = 17
Total	21	21/21*360 = 360

After calculating the required sample points for each class, the stratified random procedure was implemented to allocates those points in each classified LULC using the Sampling Design Tool in ArcGIS. Then the allocated points over the classified image were verified individually with the location of the original image to find out the number of correctly classified pixels (Ruppert, et al. 2018). Then, every point of each stratum was checked with the visual interpretation whether those are matched with the location of the original imagery. The reference points were recorded against the classified points in the attribute table to compute the confusion matrix. The matrix provided the correctly classified and misclassified pixels, Producer's Accuracy (PA), User Accuracy (UA), Overall Accuracy (OA) and Kappa statistics (Anand & Bank, 2018). Then the, error of omission and commission was calculated based on those statistics. The whole classified map, as well as each LULC category, were compared by evaluating all the accuracy and errors.

3. RESULT AND DISCUSSION

3.1 LULC 2020

The metropolitan city is predominantly covered by forest, particularly in the northwest and southeast regions. Forest patches are noticeable at the center of the city, surrounded by agricultural land. The forested areas vary in density, with some being more spacious, attributed to natural forest cover and community-managed forests. Ongoing forest protection programs, both at the national and community levels, have led to the conversion of degraded land into forested areas (GoN, 2017). The majority of the built-up area is concentrated at the city center, with expansion occurring towards the periphery, driven largely by people's preference to settle near the east-west highway, particularly individuals migrating from outside of the city. Water bodies are primarily located at the center of the city and surrounding settlements, influenced by nearby flowing rivers and the growing interest of locals in fish farming. Bare areas consist of sand along the ridge of the riverbank, extending from north to west and into the city, as well as degraded land and dry streams sprawled across the southern part, adjacent to forests and agricultural areas. Sparse grass patches are scattered across forested and agricultural lands (Figure 3).

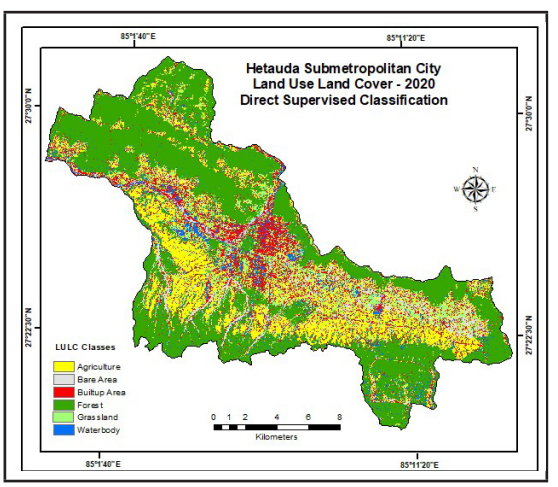

Figure 3: LULC 2020

In 2020, forest coverage was assessed at 127.8 square kilometers via direct supervised classification and 121.1 square kilometers through segment mean shift classification. Combined, forests accounted for 47.55% of the total area, emerging as the primary land cover type for the city. Agricultural land occupied 47 square kilometers in direct classification (18%) and 48 square kilometers in segment mean shift classification (18.3%). On average,

it constituted 18.15% of the total area, ranking as the second most prevalent class. Built-up areas spanned 34 square kilometers in direct classification (13%) and 32.7 square kilometers in segment mean shift classification (12.5%). Collectively, they covered 12.75% of the total area. Grasslands extended over 24.8 square kilometers in direct classification (9.5%) and 34.5 square kilometers in segment mean shift classification (13.2%). On average, they constituted 11.35% of the total area. Within the city limits, a bare area measured 14.2 square kilometers in supervised classification (5.4%) and 13.8 square kilometers in segment mean shift classification (5.3%) in 2020. Combined, it accounted for 5.35% of the total land, marking it as the second lowest land cover category. Water encompassed 13.9 square kilometers, constituting 5.3% of the total land in direct classification, and 11.7 square kilometers, accounting for 4.5% of the total land in segment mean shift classification. On average, water coverage constituted 4.9% of the total area (Table 2).

Table 2. Area coverage in direct and segment mean shift classification 2020

LULC Classes	Direct Supervised Classification		Segment Mean Shift Classification		Both Classifications (Average)	
	Area Sq Km	Per-centage	Area Sq KM	Per-centage	Area Sq KM	Per-cent-age
Agriculture	47	18	48	18.3	47.50	18.15
Bare Area	14.2	5.4	13.8	5.3	14.00	5.35
Builtup Area	34	13	32.7	12.5	33.35	12.75
Forest	127.8	48.8	121.1	46.3	124.45	47.55
Grass	24.8	9.5	34.5	13.2	29.65	11.35
Waterbody	13.9	5.3	11.7	4.5	12.80	4.9

3.2 LULC 2010 and 2020

Over the past decade, there have been significant shifts in land use patterns within the city. **Agriculture,** once the dominant sector, has seen a substantial decline from 41.68% of total land area in 2010 to 18.15% in 2020 (Figure 4). This decline is attributed to the influx of migrants from other districts and rural areas, leading to increased construction activity and the conversion of agricultural land into built-up areas. The unplanned emergence of residential areas has further contributed to the expansion of built-up areas.

Similarly, the proportion of **bare areas** decreased from 7.39% in 2010 to 5.35% in 2020 (Figure 4). This decline attributed to an increase in households and occupation by landless squatters, resulting in its conversion to either built-up or agricultural land. The fluctuating patterns of rainfall throughout the seasons cause variations in river flow, characterized by increased flow levels during the summer and reduced or dry conditions during the dry season. These fluctuations contribute to the accumulation of exposed sediments along the riverbanks when water levels recede.

Conversely, there have been notable increases in **built-up** areas, almost doubling from 6.15% in 2010 to 12.75% in 2020 (Figure 4). This expansion attributed to various factors, including the influx of migrants who seek housing opportunities in the city. Additionally, private and individual land brokers play a significant role by acquiring agricultural land and converting it into residential plots with higher resale value, thus contributing to the urban sprawl. This trend of land conversion for profit-making has persisted over the years, further exacerbating the issue. Furthermore, the rapid development of infrastructure such as the east-west highway and linking roads has facilitated urbanization by encouraging construction along roadsides. Additionally, the presence of landless squatters has led to the encroachment of land, contributing to the escalating built-up area within the city.

Grassland has experienced a substantial increase from 2.34% in 2010 to 11.35% in 2020 (Figure 4). This increase attributed to the expansion of fallow land and the implementation of community-based forest

programs within the city. Additionally, the proliferation of bushes in the area could be a consequence of illegal fires, particularly during April and May, as well as haphazard logging practices that make the forest space open for the grass

The **forest** cover has slightly increase from 41.46% in 2010 to 47.55% in 2020 (Figure 4), it remains a significant portion of the city's land area. The forest area become more spacious and dense due to existing natural forest and the conservation efforts made by the communities and the government agencies in the city. For years, forest protection programs have been diligently implemented both in national forests and community-managed forest areas. As a result of these sustained efforts, degraded lands have undergone a transformation from barren or bushy areas into thriving forests. This remarkable conversion underscores the effectiveness of conservation initiatives in restoring and regenerating forest ecosystems. By focusing on both national and local levels of forest management, these programs have played a crucial role in reclaiming degraded land and fostering the growth of vital forest habitats.

There has been a noteworthy increase in **water** bodies, rising from 0.97% in 2010 to 4.9% in 2020 (Figure 4). The rise in water bodies can be credited to the construction of ponds primarily intended for fishery purposes. The Bagmati River originates in the north and meanders westward through the heart of the city,

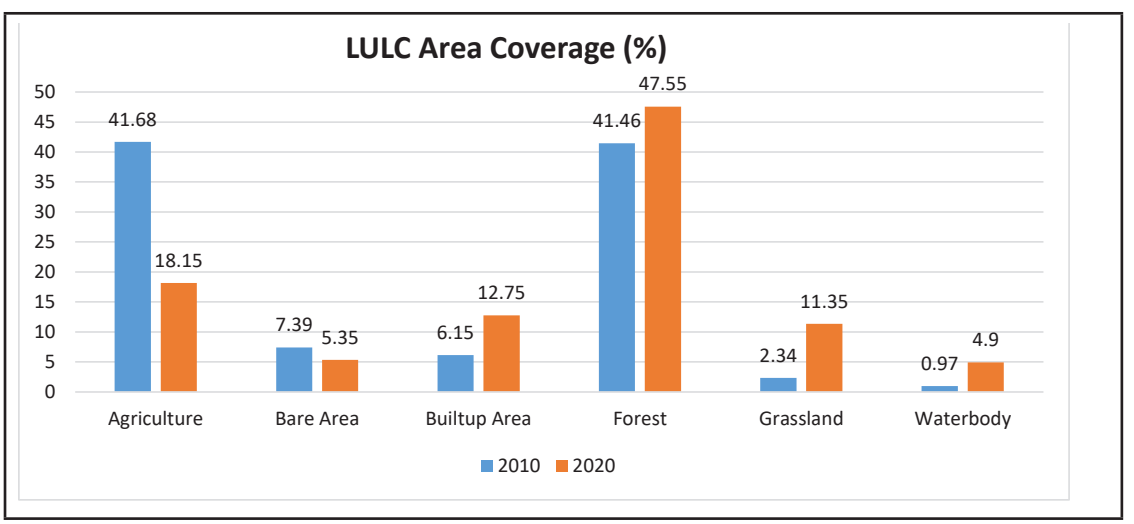

Figure 4: LULC of 2010 and 2020

3.3 Map accuracy

The accuracy of thematic maps in image classification is crucial before presenting them to users (Foody, 2013). The assessment output may vary depending on the application, but it relies on quantitative results to ascertain the map's reliability (Congalton, 2001). Thomlinson et al. (1999) suggest a minimum overall accuracy of 85%, with each class accuracy at 70%. Meeting these criteria indicates that the classified data is relatively accurate to the ground. Similarly, Anderson et al. (1992) propose an acceptable accuracy threshold of 85% for satellite land cover classifications, a similar accuracy limit echoed by Congalton (2001). Adhering to this accuracy limit, the reclassification of LULC data for the sub-metropolitan city was conducted to meet the minimum requirement. To find out the accuracy, the quantitative assessment - the confusion matrix was generated to assess how well the classification model is performing

by comparing the predicted classes with the actual classes.

3.3.1 Accuracy of LULC (Direct Supervised Classification)

Out of a total of 360 pixels, 306 are accurately classified, yielding an overall accuracy of 85% (Table 3). The classification matrix reveals specific accuracies within different land cover categories: for forests, 101 out of 103 pixels are correctly identified, resulting in 93% producer accuracy and 98% user's accuracy. Agriculture exhibits 76 out of 86 correctly classified pixels, translating to 84% producer accuracy and 88% user's accuracy. In built-up areas, 37 out of 51 pixels are correctly labeled, leading to 66% user's accuracy and 73% producer accuracy. Similarly, bare areas showcase 55 out of 69 correctly classified pixels, reflecting 92% producer accuracy and 80% user's accuracy. Lastly, waterbodies have 12 out of 17 pixels correctly identified resulting 100% producer accuracy and 71% user accuracy. The kappa statistics of 0.81 which gives the 81% reliability interprets the strong level of agreement between classified and original map (Table 3).

Table 3. Statistics of accuracy assessment (Direct Supervised Classification)

Class Value	Agriculture	Bare Area	Builtup Area	Forest	Grassland	Waterbody	Total	UA
Agriculture	76	0	6	1	3	0	86	**0.88**
Bare Area	4	25	5	0	0	0	34	**0.74**
Builtup Area	3	7	37	3	1	0	51	**0.73**
Forest	0	0	1	101	1	0	103	**0.98**
Grassland	7	0	5	1	55	0	69	**0.80**
Waterbody	0	0	2	3	0	12	17	**0.71**
Total	90	32	56	109	60	12	360	
PA	**0.84**	**0.78**	**0.66**	**0.93**	**0.92**	**1.00**		
OA								**0.85**
Kappa								**0.81**

3.3.2 Accuracy of LULC (Segment Mean Shift Classification)

Out of a total of 360 pixels, 325 are accurately classified, yielding an overall accuracy of 90% (Table 4). The classification matrix reveals specific accuracies within different land cover categories: for forests, 101 out of 103 pixels are correctly identified, resulting in 94% producer accuracy and 98% user's accuracy. Agriculture exhibits 79 out of 86 correctly classified pixels, translating to 88% producer accuracy and 92% user's accuracy. In built-up areas, 46 out of 51 pixels are correctly labeled, leading to 90% user's accuracy and 79% producer accuracy. Similarly, bare areas showcase 56 out of 69 correctly classified pixels, reflecting 98% producer accuracy and 81% user's accuracy. Lastly, waterbodies have 12 out of 17 pixels correctly identified, translating 92% producer accuracy and 71 % user accuracy. The kappa statistics of 0.88 which gives the 88 % reliability interprets the strong level of agreement between classified and original map (Table 4).

Table 4. Statistics of accuracy assessment (Segment Mean Shift Classification)

Class Value	Agriculture	Bare Area	Builtup Area	Forest	Grassland	Waterbody	Total	UA
Agriculture	79	0	1	2	4	0	86	0.92
Bare Area	4	56	8	0	0	1	69	0.81
Builtup Area	3	1	46	1	0	0	51	0.90
Forest	2	0	0	101	0	0	103	0.98
Grassland	1	0	0	2	31	0	34	0.91
Waterbody	1	0	3	1	0	12	17	0.71
Total	90	57	58	107	35	13	360	0
PA	0.88	0.98	0.79	0.94	0.89	0.92		
OA								**0.90**
Kappa								**0.88**

3.3.3 Error of omission and error of commission

In the Direct Supervised Classification of LULC classes, the error analysis reveals varying levels of accuracy across different categories. Notably, Agriculture demonstrates a moderate level of omission error at 16% and a slightly lower commission error at 12%, indicating a relatively balanced performance in classification. Conversely, Bare Area exhibits a higher omission error at 22% compared to a commission error of 26%, suggesting a tendency to miss classifying areas as bare more frequently than misclassifying into this category. Builtup Area shows a higher commission error at 27% versus an omission error of 34%, indicating a tendency to misclassify non-built areas as builtup more often. Forest demonstrates a low omission error of 7% and a very low commission error of 2%, indicating high accuracy in classification. However, Grassland presents a higher commission error at 19% and a moderate omission error at 7%, indicating a tendency to misclassify other land cover types as grassland more frequently. Waterbody shows no omission error but a high commission error of 29%, indicating a tendency to misclassify other features as water bodies (Table 5).

In the Segment Mean Shift Classification of LULC classes, the error analysis highlights fluctuations in accuracy across different categories compared to Direct Supervised Classification. Notably, there is a decrease in the error of omission for some classes, such as Bare Area with 1.75% and Builtup Area with 20.69%, indicating improved accuracy in identifying these land cover types. However, this decrease is offset by an increase in commission error, particularly evident in Bare Area with 18.84% and Builtup Area with 9.8%. Conversely, Forest demonstrates a significant decrease in commission error at 1.94% while maintaining a low omission error at 5.61%, suggesting enhanced accuracy in classifying forested areas. However, Grassland shows a relatively higher commission error at 8.82% and a moderate omission error at 11.43%, indicating a tendency to misclassify other land cover types as grassland more frequently. Waterbody exhibits a decrease in commission error at 29.41% but no change in the omission error, suggesting an improvement in accurately identifying water bodies, albeit with a higher tendency for misclassification (Table 5).

Table 5: Omission and Commission Error

Error of LULC 2020				
LULC Classes	Direct Supervised Classification)		Segment Mean Shift Classification	
	Error of Omission	Error of Commission	Error of Omission	Error of Commission
Agriculture	16	12	12.22	15.3
Bare Area	22	26	1.75	18.84
Builtup Area	34	27	20.69	9.8
Forest	7	2	5.61	1.94
Grassland	7	19	11.43	8.82
Waterbody	0	29	7.69	29.41

4. CONCLUSION

The LULC classification of Hetauda Sub-Metropolitan City, utilized both direct supervised classification and segment mean shift methods with Sentinel 2B, Level-C, orthorectified data acquired on 31 March 2020, and 10-meter spatial resolution from the European Space Agency. Geo-registration at UTM 45 N projection, atmospheric correction for noise reduction, and histogram equalization for contrast enhancement were employed. Six LULC classes were identified: forest, agriculture, built-up area, bare area, grassland, and waterbody, with forest covering the largest area at 124.45 sq km, representing 47.55% of the total city area. Agriculture, built-up, bare land, grass, and waterbody covered 18.15%, 12.75%, 5.35%, 11.35%, and 4.9% of the area, respectively. Notably, forest, water, bare area, grassland, and the built-up area have increased since 2010, while agriculture has decreased significantly. The segment mean shift supervised classification achieved an overall accuracy of 90%, outperforming the 85% accuracy of direct supervised classification, with strong agreement shown by kappa statistics at 0.88 and 0.81, respectively. The forest class demonstrated the highest accuracy at 98%, while waterbody classification exhibited the lowest reliability. Thus, the segment mean shift method emerges as the preferred choice for LULC classification, considering both appropriateness and accuracy.

REFERENCE

Ai, J., , C., Chen, L., & Li, D. (2020). *Mapping Annual Land Use and Land Cover Changes in the Yangtze Estuary Region Using an Object-Based Classification Framework and Landsat Time Series Data*.

Anand, A., & Bank, W. (2018). *Unit 14 Accuracy Assessment* (pp. 59-77). Retrieved from https://www.researchgate.net/publication/324943246_UNIT_14_ACCURACY_ASSESSMENT.

Anderson, M. L., Heigh, R. I., Mccoy, G. A., Parent, K., Muhm, J. R., Mckee, G. S., Eversman, W. G., & Collins, J. M. (1992). *Accuracy of Assessment of the Extent of Examination by Experienced Colonoscopists*. 560–563.

Basayigit, L. (2015). *Comparison of Pixel-Based and Object-Based Classification. Land Reclamation, Earth Observation & Surveying, Environmental Engineering*, (March 2018).

Belward, A. S., & Skøien, J. O. (2015). *Who Launched What, When and Why: Trends in Global Land-Cover Observation Capacity from Civilian Earth Observation Satellites*. ISPRS

Journal of Photogrammetry and Remote Sensing, 103, 115–128. https://doi.org/10.1016/j.isprsjprs.2014.03.009.

Buja, K., & Menza, C. (n.d.). *Sampling Design Tool for ArcGIS - Instruction Manual* (pp. 1–16). Retrieved from http://www.arcgis.com/home/item.html?id=ecbe1fc44f35465f9dea42ef9b63e785.

CBS. (2021). The Population and Housing Census 2021. Central Bureau of Statistics. Kathmandu. Nepal

Clarke, M. R. B., Duda, R. O., & Hart, P. E. (1974). *Pattern Classification and Scene Analysis*. Journal of the Royal Statistical Society. Series A (General), 137(3), 442. https://doi.org/10.2307/2344977.

Cohen, J. (1960). *A Coefficient of Agreement for Normal Scales. Educational and Psychological Measurement*, XX(1), 37–46. https://doi.org/10.1177/001316446002000104

Comaniciu, D., & Meer, P. (2002). *Mean Shift: A Robust Approach toward Feature Space Analysis. IEEE Transactions on Pattern Analysis and Machine Intelligence*, 24(5), 603–619. https://doi.org/10.1109/34.1000236.

Congalton, R. G. (2001). *Accuracy Assessment and Validation of Remotely Sensed and Other Spatial Information. International Journal of Wildland Fire*, 10(3–4), 321–328. https://doi.org/10.1071/wf01031.

DoA. (2018). *Inter Provincial Dependency for Agricultural Development*. Department of Agriculture. Kathmandu. Nepal

Enderle, D. I. M., & Robert, C. W. J. (2005). *Integrating Supervised and Unsupervised Classification Methods to Develop a More Accurate Land Cover Classification.* Journal of the Arkansas Academy of Science, 59, 65–73.

ESA. (2015). *SENTINEL-2 User Handbook*. Retrieved March 1, 2021, from https://sentinels.copernicus.eu/documents/247904/685211/Sentinel-2_User_Handbook.

ESA. (n.d.). *Copernicus Open Access Hub*. Retrieved November 6, 2020, from https://scihub.copernicus.eu/dhus/#/home.

ESRI. (n.d.-a). *ArcGIS.* Retrieved June 19, 2021, from https://www.esri.com/en-us/arcgis/about-arcgis/overview.

ESRI. (n.d.-b). *Mosaic Operators*. Retrieved February 19, 2021, from https://desktop.arcgis.com/en/arcmap/10.3/manage-data/raster-and-images/mosaic-operators.htm.

ESRI. (n.d.-c). *Segment Mean Shift*. Retrieved March 18, 2021, from https://pro.arcgis.com/en/pro-app/tool-reference/spatial-analyst/segment-mean-shift.htm.

ESRI. (n.d.-d). *Understanding Segmentation and Classification*. Retrieved January 8, 2020, from https://desktop.arcgis.com/en/arcmap/10.3/tools/spatial-analyst-toolbox/understanding-segmentation-and-classification.htm.

ESRI. (n.d.-e). *Understanding Segmentation and Classification*. Retrieved March 18, 2021, from https://pro.arcgis.com/en/pro-app/tool-reference/spatial-analyst/understanding-segmentation-and-classification.htm.

Food and Agriculture Organization of the United Nations [FAO]. (2016). *Map accuracy assessment and area estimation: A practical guide (National Forest Monitoring Assessment*, Working Paper No. E(46)). Retrieved from http://www.fao.org/3/a-i5601e.pdf.

Foody, G. M. (2013). *Thematic Map Comparison. Photogrammetric Engineering & Remote Sensing*, 70(5),

627–633. https://doi.org/10.14358/pers.70.5.627.

Government of Nepal; Office of the Hetauda Sub-Metropolitan City[GoN]. (2017). *City Profile of Hetauda Sub-Metropolitan City*, 2017 (Vol. २०७४).

Hegarty-Craver, M., Polly, J., Neil, M. O., Ujeneza, N., Rineer, J., Beach, R. H., Lapidus, D., & Temple, D. S. (2020*). Remote Crop Mapping at Scale: Using Satellite Imagery and UAV-Acquired Data as Ground Truth*. Remote Sensing, 1–15.

Intergraph; Erdas. (2021). *Top 10 Reasons to Use ERDAS IMAGINE*, 8–9. Retrieved June 19, 2021, from https://www.esri.com/en-us/arcgis/about-arcgis/overview.

Lillesand, T. M., Kiefer, R. W., & Chipman, J. (2015). *Remote Sensing and Image Interpretation* (7th ed.). Vol. 53(9), 1689-1699.

McHugh, M. L. (2012). *Lessons in Biostatistics: Interpreter Reliability: The Kappa Statistic*. 276–282. https://doi.org/10.11613/BM.2012.031

MGL. (n.d.). *Accuracy Assessment of an Image Classification in ArcMap* [Video file]. Retrieved from Library. https://www.youtube.com/watch?v=FaZGAUS_Nlo&t=699s.

Phiri, D., & Morgenroth, J. (2017). *Developments in Landsat Land Cover Classification Methods: A Review*. Remote Sensing, 9(9), 967. https://doi.org/10.3390/rs9090967.

Roy, P. S., Behera, M. D., & Srivastav, S. K. (2017). *Satellite Remote Sensing: Sensors, Applications and Techniques. Proceedings of the National Academy of Sciences India Section A: Physical Sciences*, 87(4), 465–472. https://doi.org/10.1007/s40010-017-0428-8.

Ruppert, G., Hussain, M., & Heimo, M. (2018). *Accuracy Assessment of Satellite Image Classification Depending on Training Sample*. Journal Name, 28(4), 195–201.

Thomlinson, J. R., Bolstad, P. V., & Cohen, W. B. (1999). *Coordinating Methodologies for Scaling Landcover Classifications from Site-Specific to Global: Steps toward Validating Global Map Products*. (Report No. 4257(99).

Viera, A. J., & Garrett, J. M. (2005). *Understanding Interobserver Agreement: The Kappa Statistic*. 360–363.

Author's Information

Name	:	Menaka Hamal
Academic Qualification	:	MSc in Natural Resource Management
Organization	:	Nutan GeoEnvironmental Consultancy Pvt. Ltd
Current Designation	:	Managing Director
Work Experience	:	13 years
Published paper/article	:	5